Austempering Time and Its Influence on the Mechanical Performance of Inverse Bainite: Insights from Hardness, Toughness, and Strength Testing

Aqil Inam, Waqas Dilawar, Muhammad Haseeb Hassan, Faraz Hussain, Inam Ullah, Muhammad Ishtiaq*
Institute of Metallurgy & Materials Engineering, University of the Punjab, 54590, Lahore, Pakistan
*Correspondence: Muhammad Ishtiaq ishtiaq.imme@pu.edu.pk,

Citation | Inam. A., Dilawar. W., Khan., Hassan. M. H, Hussain. F, Ullah. I, Ishtiaq.M.,"Austempering Time and Its Influence on the Mechanical Performance of Inverse Bainite: Insights from Hardness, Toughness, and Strength Testing", IJIST, Vol. 06 Issue. 04 pp 1932-1942, Nov 2024
Received | Oct 25, 2024 **Revised |** Nov 17, 2024 **Accepted |** Nov 20, 2024 **Published |** Nov 22, 2024.

This study examines the impact of austempering time on the mechanical properties of 0.8C experimental steel with inverse bainitic microstructures. Samples were austenitized at 900 °C and austempered at 420 °C for 30, 60, 90, and 120 minutes. The effects on hardness, impact toughness, and (UTS) were analyzed. Microstructural evaluations by optical microscope, scanning electron microscope, and energy dispersive spectroscopy confirmed the formation of inverse bainite. Mechanical testing showed that increasing austempering time leads to higher hardness due to cementite lath growth and reduced ferrite content, but also results in lower Charpy impact energy, indicating reduced toughness. While UTS initially decreases, it increases sharply after 120 minutes, accompanied by brittle fracture. This study suggests that prolonged austempering enhances hardness and strength but increases brittleness, making these structures less suitable for applications involving sudden forces.

Ultimate Tensile Strength	(UTS)
Scanning Electron Microscopy	(SEM)
Body-Centered Cubic	(BCC)
Face-Centered Cubic	(FCC)
Transformation-Induced Plasticity	(TRIP)
Bainitic Start Temperature	(Bs)
Martensitic Start Temperature	(Ms)

Keywords: Inverse Bainite, Austempering Time, Hardness, Impact Strength; Mechanical Properties.

Introduction:

A conventional heat treatment process known as intercortical annealing is employed to produce ferritic-bainitic microstructures with enhanced mechanical properties. In hypo-eutectoid steels, this treatment results in the formation of bainite, while in hyper-eutectoid steels, the eutectoid transformation leads to the development of inverse bainite. In bainite, the eutectoid transformation primarily involves the nucleation of ferrite from the parent austenite. In contrast, inverse bainite sees cementite nucleate first from the parent austenite, followed by the formation of ferrite [1]. Author's proposal [1], research on inverse bainite has been limited. Existing studies mainly focus on identifying and understanding its microstructure [2][3][4], exploring the diffusion of various elements during transformation [5][6], and investigating its morphology [6][7] and resulting mechanical properties [8][9]. TEM studies conducted by [2] demonstrated that in inverse bainite, cementite initiates nucleation first, with ferrite subsequently forming at the interface between the pro-eutectoid cementite and austenite. In [10] regarded the bainitic transformation in hypereutectoid steel as a diffusion-displacive-controlled transformation. Isothermal bainite transformation is associated with notable volumetric expansion, as evidenced by numerous studies employing dilatometry to assess bainitic transformation [11][12].

Hypereutectoid steels find extensive applications in cutting tools [13], bearings [14], springs [15], rails, dies, molds [16], and armor plates [17], which has prompted significant research into their properties and performance. Most research has concentrated on evaluating the microstructure, with no comprehensive studies, to our knowledge, on the effect of austempering temperature and/or time on the final mechanical properties of inverse bainite. Although there are several studies on the mechanical properties of bainite. For example, [18] observed that raising the austempering temperature from 180 °C to 260 °C increased the bainite content from 3.5% to 36.1%. They also found that increasing the temperature led to a decrease in both the hardness and impact strength of the steel. This reduction was attributed to the weakening of dispersion strengthening, which was linked to the growth of carbide particles. A comparable study by [19] examined the impact of austempering temperature on the microstructure and mechanical properties of 0.7C steel. They reported that as the austempering temperature increased, the volume fraction of retained austenite also rose, leading to an improved combination of strength and ductility [20] reported that increasing the austempering time resulted in a higher yield strength. However, no significant effect was observed on microhardness. This variation was attributed to differences in the quantities of constituents formed during the isothermal treatment. Specifically, high hardness values were associated with the presence of martensite, while lower values reflected the influence of bainite and retained austenite. The increase in yield strength was due to the significant presence of martensite and bainite sheaves. A recent study by [21] examined the impact of austempering time on the mechanical properties of low-carbon steels and reported that extending the austempering time led to an increase in yield strength, which was linked to a higher amount of retained austenite with elevated carbon content.

Detailed studies on the effect of austempering time on the mechanical properties of hypereutectoid steel with an inverse bainite morphology are currently lacking. Therefore, this study aims to investigate how varying austempering times impact the mechanical properties of 0.8C hypereutectoid experimental steel. The research includes heat treatment, microstructural evaluation, and assessments of mechanical properties through hardness testing, tensile testing, and impact testing. The goal is to enhance the understanding of these materials and improve their utilization in engineering applications.

Materials and Methods:

Materials: A hypereutectoid steel composition with 0.8% carbon was selected to facilitate the formation of inverse bainite [4][22]. The steel used in this study was sourced from New Shalimar

Steel (Pvt.) Limited, Lahore, Pakistan. A total weight of 20 kg was produced in an induction furnace using steel scrap. The steel was initially cast into ingots, which were subsequently hot-rolled into sheets with a thickness of approximately 10 mm. The chemical composition of the prepared steel was analyzed using an emission spectrometer, and the results are detailed in Table 1.

Table 1. Chemical composition (wt.%) of the experimental Steel

Element	C	Si	Mn	P	S	Cr	Ni
Wt.%	0.81	0.97	1.60	0.07	0.03	0.84	1.16

For mechanical testing, dog-bone-shaped samples were wire-cut from the steel sheets in compliance with ASTM E-8 standards. Charpy V-notch impact samples were also prepared from the 10 mm thick plate using wire cutting, following ASTM E23 standards. Additionally, round samples of ~ 12 mm diameter were cut from steel rods using a disc cutter for heat treatment and metallographic analysis. Following the cutting process, the samples underwent a cleaning procedure to remove grease, rust, oil, and other contaminants from their surfaces. Once cleaned, the surfaces were rough-ground with P100-grade grinding paper to eliminate scale. To facilitate handling, specimens were secured with Ni-Chrome wire.

Heat treatment:

The austempering heat treatment was conducted on the experimental steels using salt-bath furnaces. The samples were austenitized at 900 °C for 30 minutes (1800 seconds) in an electric muffle furnace. The austempering temperature was meticulously chosen to lie between the (Bs) and the (Ms). This selection ensured the formation of bainite while preventing the formation of martensite. The Bs and Ms temperatures were calculated using empirical equations 1[23]and 2 [24].

$$Bs\ (°C) = 656 - 57.7C - 75Si - 35Mn - 15.3Ni - 34Cr - 41Mo \quad (1)$$

$$Ms\ (°C) = 539 - 432C - 30.4Mn - 17.7Ni - 12.1Cr - 7.5Mo \quad (2)$$

By substituting the composition into equations (1) and (2), we obtained a Ms temperature of 412 °C and a Bs temperature of 435 °C. Therefore, an intermediate temperature of 420 °C was selected for the austempering process. After austenitizing, the specimens were quickly transferred to a salt bath composed of 50% KNO_3 and 50% $NaNO_3$, which was maintained at 420 °C. The specimens were then tempered for 30, 60, 90, and 120 minutes before being air-cooled. The heat treatment cycle is illustrated in Figure 1.

Metallography:

The heat-treated samples were initially rinsed with water to eliminate any residual salt from their surfaces. Following this, any remaining scale was carefully removed using P100-grade grinding paper. The specimens were then mounted in Bakelite powder using a Buehler automatic mounting press set at 1000 psi. Once mounted, the samples underwent standard grinding and polishing procedures to achieve a smooth, uniform surface. For microstructural analysis, the polished samples were etched with a 2% Nital solution (2% HNO_3 in 98% ethanol)o, which facilitated the examination of their microstructure.

Microscopy:

Light optical microscopy was performed using a Leica DM 15000 M research microscope, equipped with a digital camera for detailed imaging of the specimens' microstructures. For (SEM), microstructural images were obtained using an FEI Inspect S-50 microscope operated at 15 kV to capture detailed surface features and morphology of the heat-treated samples.

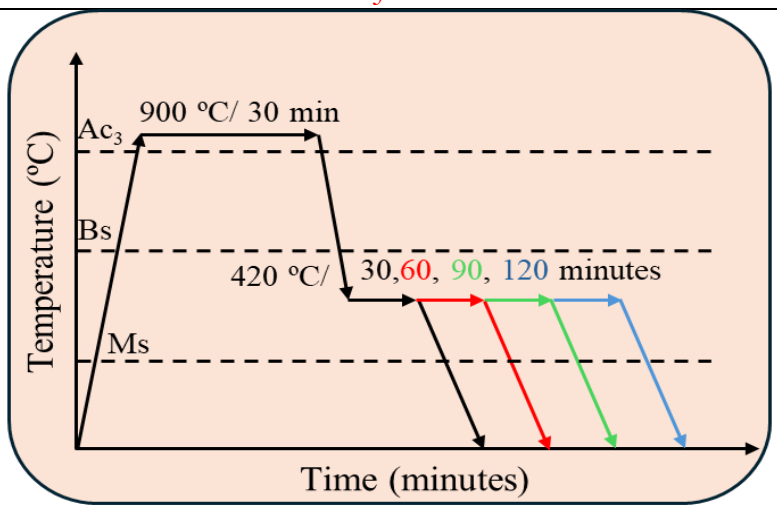

Figure 1. Austempering heat cycle adopted for experimental steel.

Mechanical Testing:

The Vickers hardness of the heat-treated samples was measured using a Shimadzu Micro-Hardness Tester. Charpy impact tests were conducted on V-notch specimens using a 300 J ZBC2152 metal pendulum impact machine. Tensile testing was performed at room temperature using a 300 kN electromechanical tensile testing machine. Three readings for each test were taken per sample, and the average value was calculated to ensure consistency.

Results and Discussion:

Optical Microscopy:

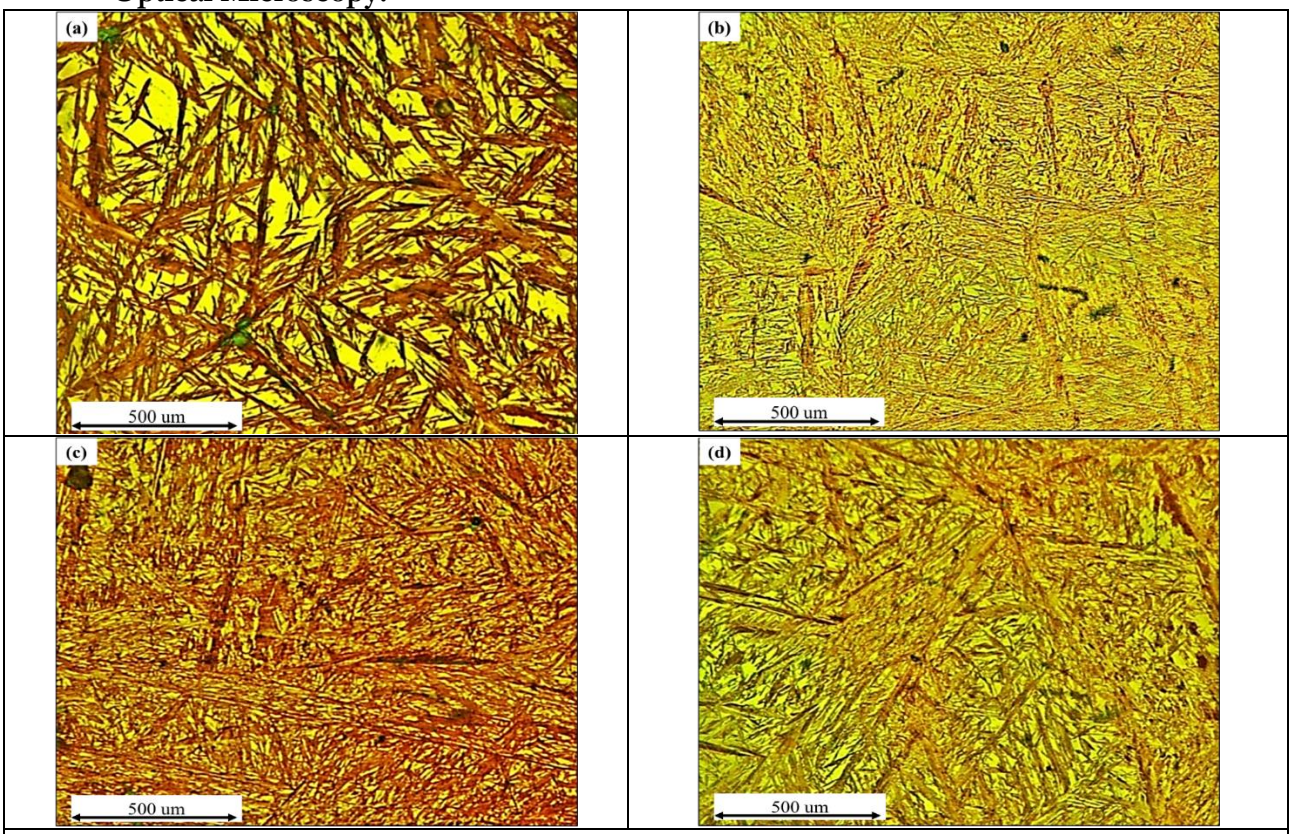

Figure 2.Optical micrographs showing inverse bainite morphologies in 0.8% C after an austempering time of (a) 30 min (b) 60 min (c) 90 min (d) 120 min. 2% Nital etched

Light optical metallographic images of the 0.8C experimental steel exhibiting inverse bainitic microstructures after austempering heat treatment for different time intervals are

presented in Figure 2. As-received or annealed state, the steel initially exhibits a ferrite-pearlite structure. However, upon cooling from the austenitizing temperature of 900 °C to the austempering temperature of 420 °C, the structure transforms into inverse bainite. This transformation occurs due to the supersaturation of cementite in the austenite, which results in the formation of Widmanstätten cementite plates. This alteration disrupts the eutectoid structure, thereby promoting the development of inverse bainite [25]. Figure 2(a) shows the microstructure of a specimen austempered for 30 minutes, revealing a lath-like arrangement of cementite within the bainitic ferrite matrix. This microstructure should be classified as inverse bainite, as cementite appears to be the primary nucleating phase, unlike the ferrite-dominant phase seen in conventional bainite. Inverse bainite is characterized by the nucleation of acicular units within the austenite grains, which then grow in multiple directions, resulting in the formation of spiky nodules as shown in Figure 2(a). A similar observation of inverse bainite is evident in the images shown in Figure 2(b-d) corresponding to longer austempering durations of 60, 90, and 120 minutes, respectively. Notably, the cementite laths become finer and longer with increased austempering time, while the white areas representing ferrite become smaller overall.

Scanning Electron Microscopy:

Figure 3 presents SEM images of 0.8C experimental steel austempered to develop an inverse bainitic structure for various austempering times. In these images, small midribs with higher carbon content at the center, identified as cementite, are surrounded by ferrite. This feature, characteristic of inverse bainite where cementite is the primary nucleating phase, is evident across all austempering conditions shown in Figure 3 (a-d). These SEM images provide an overview at lower magnification; for further confirmation, a higher magnification image is used for SEM-EDS analysis. Since the primary focus of this paper is on the effect of austempering time on mechanical properties, detailed microstructural identification and evaluation are beyond its scope. Consequently, high-magnification SEM and/or TEM images are not provided in this study.

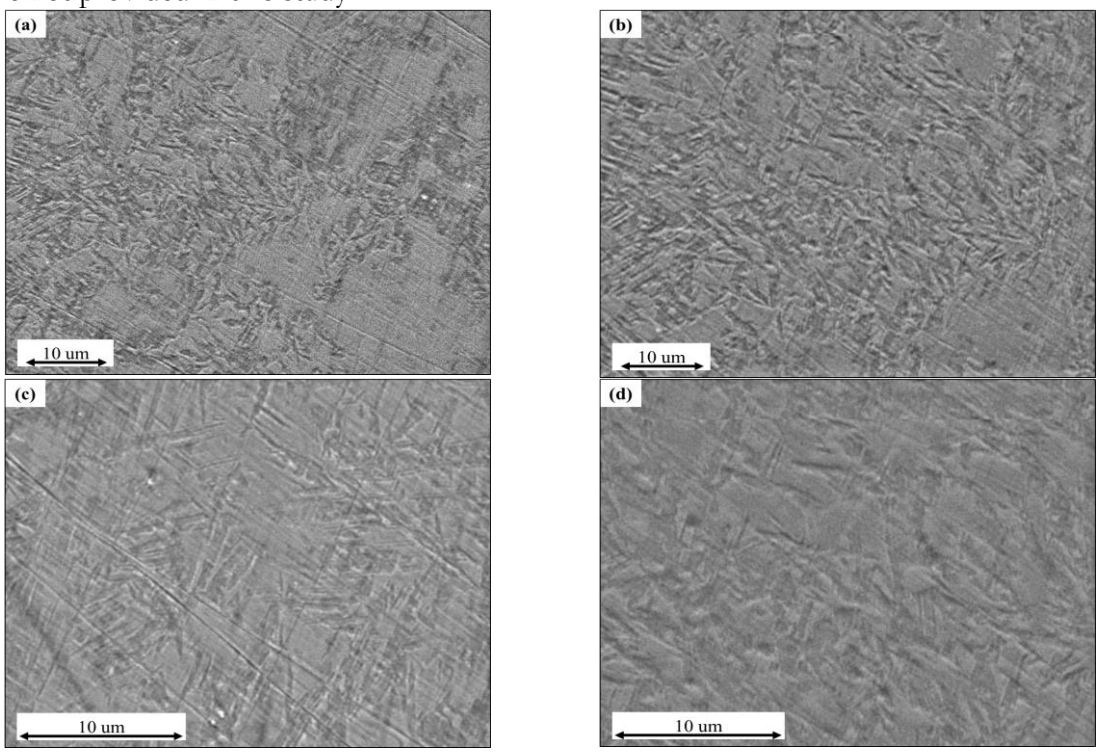

Figure 3. SEM micrographs showing inverse bainite morphologies in 0.8% C after an austempering time of (a) 30 min (b) 60 min (c) 90 min (d) 120 min. 2% Nital etched.

SEM-EDS Spot Analysis:

SEM-EDS analysis was performed at three specific locations, as highlighted in Figure 4, to identify the inverse bainite microstructure, which includes cementite midribs, ferrite, and retained austenite. The accompanying table details the carbon concentrations at each of these points, confirming the presence of these phases.

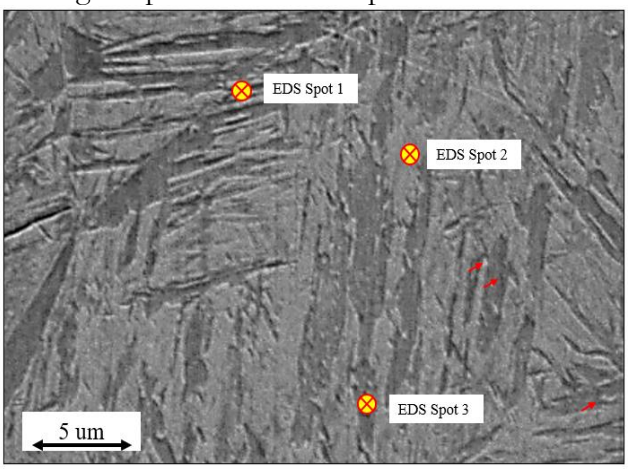

Element	Spot 1	Spot 2	Spot 3
	Wt.%		
C K	6.21	1.02	4.22
Mn L	4.74	3.05	4.81
Si K	0.84	0.63	1.03
Fe K	88.20	95.06	89.78

Figure 4. SEM micrograph of 0.8%C experimental steel austempered for 30 minutes, with EDS spot analysis conducted at three distinct locations. The spots correspond to areas potentially containing cementite, ferrite, and retained austenite. Red arrows are pointing towards very small areas potentially retained austenite.

Spot 1, with a carbon concentration of 6.21%, corresponds to cementite, known for its high carbon content and hardness. This suggests that Spot 1 represents a cementite midrib, a typical feature in the microstructure of austempered steel. Spot 2, with a carbon concentration of 1.02%, closely relates to the composition of ferrite, a softer and more ductile phase with a (BCC) structure and low carbon content. Spot 3, showing a carbon concentration of 4.22%, indicates transition carbide. It might also be retained austenite, a phase stabilized by its higher carbon content and (FCC) structure, which allows it to persist at room temperature [26]. This retained austenite is enriched with carbon because the bainite formation rejects carbon, which diffuses into the nearest austenite, enhancing its stability. Retained austenite enhances the steel's impact toughness and ductility. These SEM-EDS analyses provide a comprehensive understanding of the microstructure of the austempered 0.8C experimental steel, illustrating the significant impact of the austempering process on the distribution and characteristics of cementite midribs, ferrite, and retained austenite, and consequently, on the steel's mechanical properties and overall performance.

Micro Vickers hardness:

The hardness of the inverse bainite is initially lower than that of the ferrite-pearlite structure in the as-received sample. However, as indicated by the bar graph in Figure 5, the hardness increases with longer austempering times. Specifically, the hardness of the inverse bainite formed after 120 minutes of austempering is significantly higher than that of the steel austempered for 30 minutes.

This increase in hardness with extended austempering time can be attributed to two main factors. Firstly, the size of the cementite laths increases with longer austempering durations. Larger cementite laths contribute to higher hardness due to their inherent brittleness and strength compared to ferrite. Secondly, the content of ferrite, which is a softer phase, decreases as the austempering time increases. This reduction in ferrite content means that the proportion of harder phases, such as cementite, is higher, contributing to the overall increase in hardness. Additionally, the extended austempering time facilitates greater carbon diffusion out of ferrite, leading to the formation of carbon-rich carbides, as previously reported in

hypereutectoid steel by atom probe analysis [27]. These carbides further enhance the hardness and UTS values. These microstructural changes collectively improve the mechanical properties of the inverse bainitic steel.

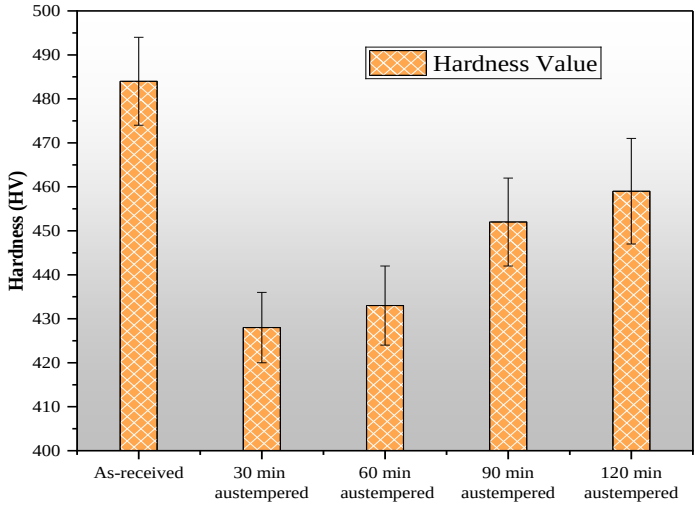

Figure 5. Bar chart showing the effect of austempering times on the Vickers hardness of 0.8C experimental steel

Impact toughness by Charpy test:

The Charpy impact properties at a constant austempering temperature of 450 °C, but with varying austempering times from 30 to 120 minutes, are presented in the graph shown in Figure 6. As anticipated, the energy absorbed decreases with increased austempering time. Specifically, the samples austempered for 30 minutes exhibit the highest energy absorption, which then declines with longer austempering durations. However, it is noteworthy that the samples austempered for 30 and 60 minutes still demonstrate better toughness compared to the as-received samples.

The decrease in Charpy impact energy with extended austempering time can be attributed to several factors. Firstly, prolonged austempering leads to the coarsening of cementite laths, which increases the steel's brittleness. Additionally, the reduction in ferrite content, a softer and more ductile phase, contributes to the decreased toughness. Ferrite helps absorb impact energy and impede crack propagation; with less ferrite, the material loses some of its ability to deform plastically under impact, resulting in lower toughness. These results indicate that the inverse bainitic structure, especially when achieved with longer austempering times, is not ideal for applications subjected to sudden impacts or forces [28].

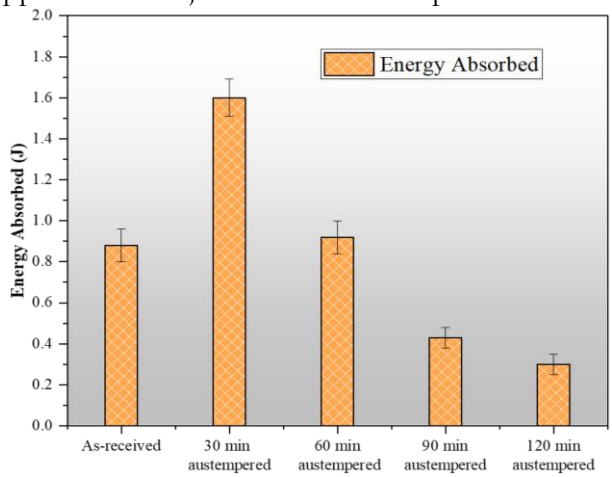

Figure 6. Bar chart showing the effect of austempering times on the toughness of 0.8C experimental steel

Tensile Testing:

Figure 7 illustrates the UTS across different austempering temperatures. The comparative analysis of UTS values across various austempering durations, reveals that the tensile strength initially decreases from the 30-minute to the 90-minute austempering times due to the predominance of ferrite over fine cementite laths. In contrast, the 120-minute austempered steel shows the highest UTS due to the presence of coarser cementite laths and the formation of carbon-rich carbides [27]. However, this also increases crack propagation and brittleness, illustrating a trade-off between strength and ductility.

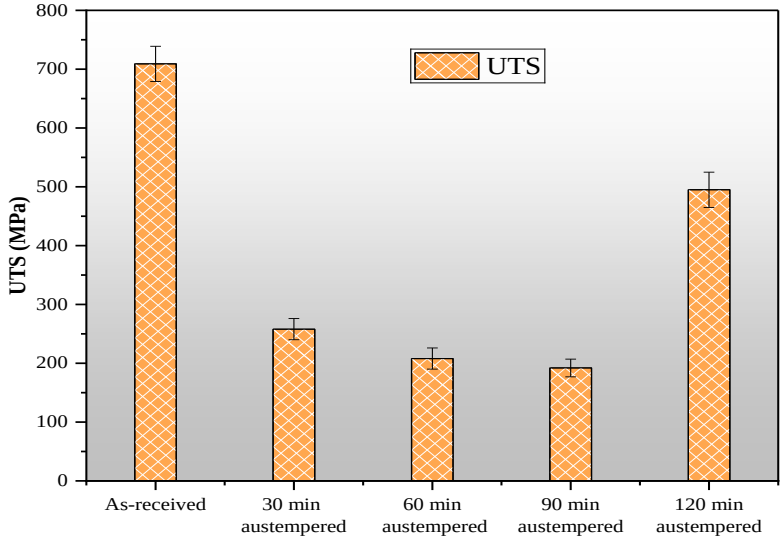

Figure 7. Bar chart showing the effect of austempering times on UTS of 0.8C experimental steel.

The increased hardness and UTS observed after longer austempering times may also be attributed to the transformation of retained austenite into martensite during final quenching. Although martensite was not detected in the initial microstructure, it is possible that deformation during tensile or hardness testing induced martensitic transformation, a phenomenon commonly known as (TRIP) [29]. This transformation could contribute to the higher hardness and UTS observed, potentially linking it to the presence of martensite formed during testing.

Conclusions:

The optical and scanning electron microscopy confirmed the formation of inverse bainite microstructure in 0.8C steel after applied heat treatment. The following conclusions are drawn from this study;

- As tempering time increased, the width of cementite plates grew, leading to a decrease in the uniformity of cementite and ferritic morphology.
- Vickers hardness values increased with an increase in austempering time.
- Charpy impact testing showed a decrease in impact energy with an increased austempering duration.
- UTS values initially decreased with longer austempering times (up to 90 minutes). However, a notable increase in UTS was observed at 120 minutes, although this came with a reduction in impact energy absorption.

Consequently, while extended austempering times can enhance hardness and UTS, they also reduce ductility, limiting the suitability of steel for applications requiring high impact resistance.

Acknowledgment:

The authors would like to thank New Shalimar Steel (Pvt.) Limited, Lahore, Pakistan for providing the steel samples for this research.

Funding:

This research did not receive any specific grant from funding agencies in the public, commercial, or not-for-profit sectors.

Author's Contributions:

All authors contributed to this research. Material preparation, data collection, and analysis were performed by Aqil Inam. The first draft of the manuscript was written by Muhammad Ishtiaq and all authors commented on previous versions of the manuscript. All authors read and approved the final manuscript.

Ethics declarations:

Declaration of Competing Interest:

The authors declare that they have no known competing financial interests or personal relationships that could have appeared to influence the work reported in this paper.

References:

[1] M. Hillert, "The role of interfacial energy during solid-state phase transformations," *Jernkontorets Ann.*, vol. 141, pp. 757–789, 1957.

[2] H. I. Kinsman, K.R., Aaronson, "The inverse bainite reaction in hypereutectoid Fe-C alloys.," *Metall. Trans.*, vol. 1, pp. 1485–1488, 1970, doi: https://doi.org/10.1007/BF02900291.

[3] A. H. I. Lee, H.J., G. Spanos, G.J. Shiflet, "Mechanisms of the bainite (non-lamellar eutectoid) reaction and a fundamental distinction between the bainite and pearlite (lamellar eutectoid) reactions," *Acta Metall.*, vol. 36, no. 4, pp. 1129–1140, 1988, doi: https://doi.org/10.1016/0001-6160(88)90166-6.

[4] S. M. H. Ishtiaq Muhammad, Aqil Inam, Hassan Munir, "Development and characterization of lower, upper, and inverse bainite in an experimental 0.8wt.% C steel," *J. Pakistan Inst. Chem. Eng.*, vol. 51, no. 2, 2024, doi: 10.54693/piche.05225.

[5] A. S. Helio Goldenstein, J.A.B. Cifuentes, "Non classical eutectoid decomposition products morphologies in Fe-Cr-C and Fe-Cr-Mo-C steels," *Solid-Solid Phase Transform. Inorg. Mater.*, 2005.

[6] H. G. & J. A. Cifuentes, "Overall kinetics and morphology of the products of austenite decomposition in a Fe-0.46 Pct C-5.2 Pct Cr alloy transformed isothermally above the bay," *Metall. Mater. Trans. A*, vol. 37, pp. 1747–1755, 2006, doi: https://doi.org/10.1007/s11661-006-0117-8.

[7] Y. W. & L. L. Rangasayee Kannan, "Microstructural Evolution of Inverse Bainite in a Hypereutectoid Low-Alloy Steel," *Metall. Mater. Trans. A*, vol. 48, pp. 6038–6054, 2017.

[8] K. S. Abbaszadeh Khodamorad, Saghafian Hassan, "Effect of Bainite Morphology on Mechanical Properties of the Mixed Bainite-martensite Microstructure in D6AC Steel," *J. Mater. Sci. Technol.*, vol. 28, no. 4, pp. 336–342, 2012, doi: https://doi.org/10.1016/S1005-0302(12)60065-6.

[9] c. H. Y. &H. K. D. H. Bhadeshia, "Strength of mixtures of bainite and martensite," *Mater. Sci. Technol.*, vol. 10, no. 3, pp. 209–214, 1994, doi: https://doi.org/10.1179/mst.1994.10.3.209.

[10] P. K. & A. Borgenstam, "Eutectoid Transformations in 4.12 Mass Pct Cr 0.88 Mass Pct C Steel," *Metall. Mater. Trans. A*, vol. 42, pp. 3941–3951, 2011, doi: https://doi.org/10.1007/s11661-011-0794-9.

[11] M. G. M. S. P.-D. R. & J. S. F. P. C. Goulas Ph.D. Candidate, "Bainite Formation in Medium-Carbon Low-Silicon Spring Steels Accounting for Chemical Segregation," *Metall. Mater. Trans. A*, vol. 47, pp. 3077–3087, 2016, doi: https://doi.org/10.1007/s11661-016-3418-6.

[12] Y. W. & L. L. Rangasayee Kannan, "A dilatometric analysis of inverse bainite transformation," *J. Mater. Sci.*, vol. 53, pp. 3692–3708, 2018, doi:

https://doi.org/10.1007/s10853-017-1752-8.

[13] S. V. M. & L. N. B. V. V. Malakhov, A. N. Yartsev, T. A. Buyanskaya, "Use of hypereutectoid high-speed steel 11M5F for the production of cutting and cold-stamping tools in the Avtovaz Joint-Stock Company," *Met. Sci. Heat Treat.*, vol. 39, pp. 186–189, 1997, doi: https://doi.org/10.1007/BF02467281.

[14] J. G. & L. H. Zhihui Chen, "Bainite Transformation Characteristics of High-Si Hypereutectoid Bearing Steel," *Metallogr. Microstruct. Anal.*, vol. 7, pp. 3–10, 2018, doi: https://doi.org/10.1007/s13632-017-0410-5.

[15] C. C. Kui Chen, Zhouhua Jiang, Liu Fubin, Jia Yu, Li Yang, Wei Gong, "Effect of quenching and tempering temperature on microstructure and tensile properties of microalloyed ultra-high strength suspension spring steel," *Mater. Sci. Eng. A*, vol. 766, p. 138272, 2019, doi: https://doi.org/10.1016/j.msea.2019.138272.

[16] F. Q. Ze-Ju Bao1, Hong-Yu Yang , Bai-Xin Dong , Fang Chang , Chuan-De Li , Ying Jiang, Liang-Yu Chen, Shi-Li Shu , Qi-Chuan Jiang, "Development Trend in Composition Optimization, Microstructure Manipulation, and Strengthening Methods of Die Steels under Lightweight and Integrated Die Casting," *Mater.*, vol. 16, no. 18, p. 6235, 2023, doi: 10.3390/ma16186235.

[17] D. M. Fras, Teresa, Christian C. Roth, "Fracture of high-strength armor steel under impact loading," *Int. J. Impact Eng.*, vol. 111, pp. 147–164, 2018, doi: https://doi.org/10.1016/j.ijimpeng.2017.09.009.

[18] J. D. Su, Y., S. Yang, X.F. Yu, C.B. Zhou, Y.B. Liu, X.C. Feng, Q. Zhao, Wu, "Effect of Austempering Temperature on Microstructure and Mechanical Properties of M50 Bearing Steel," *J. Mater. Res. Technol.*, vol. 20, pp. 4576–4584, 2022, doi: https://doi.org/10.1016/j.jmrt.2022.09.002.

[19] J. Zhao, "Effects of austempering temperature on bainitic microstructure and mechanical properties of a high-C high-Si steel," *Mater. Sci. Eng. A*, vol. 742, pp. 179–189, 2019, doi: https://doi.org/10.1016/j.msea.2018.11.004.

[20] D. B. S. J. A. Cruz Jr., T. F. M. Rodrigues, V. D. C. Viana, H. Abreu, "Influence of Temperature and Time of Austempering Treatment on Mechanical Properties of SAE 9254 Commercial Steel," *Steel Res. Int.*, vol. 83, no. 1, pp. 22–31, 2012, doi: https://doi.org/10.1002/srin.201100174.

[21] Q. Y. & X. C. Man Liu, Guang Xu, Jun-yu Tian, "Effect of austempering time on microstructure and properties of a low-carbon bainite steel," *Int. J. Miner. Metall. Mater.*, vol. 27, pp. 340–346, 2020, doi: https://doi.org/10.1007/s12613-019-1881-y.

[22] Y. W. & L. L. Rangasayee Kannan, "Identification of Inverse Bainite in Fe-0.84C-1Cr-1Mn Hypereutectoid Low Alloy Steel," *Metall. Mater. Trans. A*, vol. 48, pp. 948–952, 2017, doi: https://doi.org/10.1007/s11661-016-3924-6.

[23] J. G. A. R. Marder, "Phase Transformations in Ferrous Alloys," *Metall. Soc. AIME*, p. 411, 1984.

[24] A. K. W, "Empirical formulae for the calculation of some transformation temperatures," *J. Iron Steel Inst.*, vol. 203, no. 7, pp. 721–727, 1965.

[25] A. S. & J. Å. Annika Borgenstam, Peter Hedström, Mats Hillert, Peter Kolmskog, "On the Symmetry Among the Diffusional Transformation Products of Austenite," *Metall. Mater. Trans. A*, vol. 42, pp. 1558–1574, 2011, doi: https://doi.org/10.1007/s11661-010-0539-1.

[26] G. H. G.G. Ribamar, J.D. Escobar, A. Kwiatkowski da Silva, N. Schell, J.A. Ávila d, A.S. Nishikawa, J.P. Oliveira, "Austenite carbon enrichment and decomposition during quenching and tempering of high silicon high carbon bearing steel," *Acta Mater.*, vol. 247, p. 118742, 2023, doi: https://doi.org/10.1016/j.actamat.2023.118742.

[27] L. L. Rangasayee Kannan , Yiyu Wang , Jonathan Poplawsky , Sudarsanam Suresh

Babu, "Cascading phase transformations in high carbon steel resulting in the formation of inverse bainite: An atomic scale investigation," *Sci Rep*, vol. 9, no. 1, p. 5597, 2019, doi: 10.1038/s41598-019-42037-9.

[28] S. T. Watanabe, Tadao, "Toughening of brittle materials by grain boundary engineering," *Mater. Sci. Eng. A*, vol. 387–389, pp. 447–455, 2004, doi: https://doi.org/10.1016/j.msea.2004.01.140.

[29] K. K. Takashi Matsuno, Tomohiko Hojo, Ikumu Watanabe, Ayumi Shiro, Takahisa shobu, "Tensile deformation behavior of TRIP-aided bainitic ferrite steel in the post-necking strain region," *Sci. Technol. Adv. Mater. Methods*, vol. 1, no. 1, pp. 56–74, 2021, doi: https://doi.org/10.1080/27660400.2021.1922207.